Phase Delay Measurements Acquired from DSN and KSC Site Test Interferometers: Updated Study

David D. Morabito*

ABSTRACT. — Site Test Interferometers (STIs) have been operating at the three Deep Space Network (DSN) tracking sites and Kennedy Space Center (KSC) to gather statistical data on spatial phase fluctuations induced by the atmosphere. Such data are useful for characterizing the suitability of each site to host potential antenna uplink arrays at high-frequency bands (e.g., Ka-band) for telecommunications and navigation applications. As part of the effort, the phase-delay statistics are characterized on a monthly and annual basis. The data acquired include 13 full years for Goldstone Apollo (2011–2023), 12 years for Canberra (2012–2023) (with some partial months in 2011), 9 full years and 3 months for Madrid (2014–2023), and 8 years and 8 months for KSC (2014–2022). Thus, phase-delay statistics were derived from STI data spanning 2011 to 2023. This study is a continuation of the previous study that analyzed single-baseline STI phase-delay statistics acquired up to 2018. In addition to analyzing phase-delay statistics up to 2023, this current study also intercompares phase-delay statistics for all applicable periods where three simultaneous baselines were operating at the sites, and then compares the results with a theoretical model. A short period of temporal phase delay over all three baselines was examined against local wind speed and direction data providing two-dimensional correlation results.

I. Introduction

Until recently, space communications have relied primarily on lower frequency bands such as S-band (2.3 GHz) and X-band (8.4 GHz). However, these frequency bands are limited in bandwidth and thus limited in data rate. Given the desire and necessity to transition to higher data rates, higher frequency bands are being used increasingly for downlink. These bands include the deep-space Ka-band (32 GHz) and near-Earth K-band (26 GHz). However, these higher frequency bands are more susceptible to degradation due to atmospheric effects. Given that NASA will be required to provide services with high availabilities (such as at 99%) at Gb/s data rates (versus current ~ Mb/s data rates), the atmospheric phase stability (time-delay fluctuations) and atmospheric attenuation of

* Communications Architectures and Research Section.

The research described in this publication was carried out by the Jet Propulsion Laboratory, California Institute of Technology, under a contract with the National Aeronautics and Space Administration (80NM0018D0004).

candidate sites are required to be well-characterized. To do so, one can use Site Test Interferometers (STIs) that continuously measure the difference in signal delay from a celestial source (usually a geostationary satellite) to two or more points on the Earth. The resulting variations in the delay differences are principally due to atmospheric turbulence of water vapor [1]. The received signal phase difference is measured on short ~1 s timescales. During postprocessing, long-period trends due to satellite motion and instrumental drift are removed. Fluctuations in the resulting phase-delay residuals are dominated by the troposphere on timescales ranging from sub-second to several hundred seconds [2]. The phase-delay statistics vary between sites due to climate, weather conditions, terrain, and altitude. These statistics also vary at any one site diurnally, seasonally, and with the passage of weather systems. The observed turbulence varies with weather and season, but its effect over ~200 m distance scales is not measurable by ordinary meteorological instruments, hence the need for this specialized instrument. The STIs provide a long-term statistical characterization of a site. The resulting statistics on phase delay will also help future or present downlink arrays determine how much of their signal energy is being (or will be) disrupted by the atmosphere in real time, and thus provide a measure of how well any atmospheric compensation process is working.

Even though an STI site and a nearby communication antenna array experience the same short- and long-term statistical delay fluctuations, the instantaneous delay as measured by the STI is generally not useful for real-time correction of delay errors in an uplink array.[1] This is because their signal targets usually lie in different locations in the sky and thus their signals pass through different parts of the turbulent media. However, statistics acquired over multi-year periods are useful for site characterization. One can employ these long-term statistics to determine the suitability of a site for hosting an array or use them in communication link budgets for current or proposed missions using an array. Operating these STIs over long periods of several years allows for acquiring sufficient data for reliable statistical site characterization, and possibly detect trends that could be indicative of climate change at a particular site. The phase fluctuations have dependency with site location and vary with weather conditions and array configuration. Thus, their statistics are useful for determining site suitability and the maximum size of an array that can operate efficiently at a given site and frequency [2].

Section II discusses previous work involving the data extracted from these instruments over the past several years. Section III presents characteristics of the four STI sites, including experimental parameters and geometric configurations. Section IV provides a discussion of statistics acquired from single-baseline phase-delay data. This study is a continuation of the previous study [3], which covered single-baseline STI phase-delay statistics acquired for years 2011 through 2018. Here, available data acquired from years 2019 through 2023 were added to the statistical database. In addition, for the first time, Section V reports on an intercomparison of phase-delay statistics from all three baselines at each site, as well as a comparison of these data with a theoretical model. Section VI discusses an example of a short temporal period of two-dimensional phase-delay

[1] For a downlink array, the array processor can calibrate for atmospheric phase fluctuations by making use of a strong reference carrier using appropriate algorithms. For uplink arrays, such compensation is not normally feasible, so the site characterization described here is more important for that case.

measurements and its correlation with local wind data. Finally, Section VII ends with concluding remarks.

II. Previous Work

Much of the information presented in this section was also presented in the previous study [3] but is repeated here (as well as updated) to preserve the references of all previous work involving these instruments. Several STI instruments were built at the Jet Propulsion Laboratory in Pasadena, California, and they are based on a design provided by the Harvard Smithsonian Center for Astrophysics (CfA). Nearly identical instruments involving three baselines were deployed in the Apollo Valley at Goldstone, California; at Canberra, Australia; at Madrid, Spain; and at Kennedy Space Center (KSC). In addition, two-element versions of this design were deployed in South Africa and West Australia to support radio astronomy activities. Other STIs have been operating at various radio astronomy sites for numerous years. The KSC STI was deployed at the site of a preliminary array demonstration involving three 12-m diameter antennas for a project known as Ka-Band Objects: Observation and Monitoring (KaBOOM) [4]. In September 2022, the KSC STI was decommissioned and the equipment sent to Goldstone for storage to be used as spare parts for the existing STIs or to be deployed at prospective array sites elsewhere in the world.

An STI instrument with a different design was developed in collaboration with the NASA Glenn Research Center (GRC) and deployed in May 2007 at Goldstone at the Venus antenna site where the research and development (R&D) 34-m antenna, Deep Space Station (DSS) 13, resides. This two-element instrument consisted of 1.2-m diameter antennas forming an interferometer of 256 m separation oriented in the east–west direction. This STI instrument operated at 20.2 GHz and continuously observed the ANIK F2 satellite at an elevation of 48.5° for several years. Details of the operation of this STI instrument are discussed elsewhere [5–10], including discussion on data processing [8] and early phase-fluctuation results [11]. The slope of the temporal structure function of the phase delay (prior to the knee) with time interval, τ, agreed very well with the thick-layer model slope $\tau^{5/3}$ during the hottest summer day, and with the thin-layer model slope $\tau^{2/3}$ during the coldest winter night at Goldstone, in agreement with the Kolmogorov model [11]. Most of the time, the resulting slope fell between these two limits. Uplink array loss was presented for sample antenna array configurations as a function of frequency and root mean square (RMS) delay fluctuation [10].

Data from two independent instruments occupying the same complex, Goldstone Apollo and the Goldstone Venus STIs, were utilized in an intercomparison study [11–12]. Both instruments were deployed to assess the suitability of Goldstone for uplink arraying and to statistically characterize the atmosphere-induced phase variations for application to future arrays. The Venus STI data and the Apollo STI data (using the east–west baseline) were examined temporally and statistically. Both instruments consist of two ~1-m diameter antennas and associated electronics separated by ~200 m. The two Goldstone STI locations were separated by 12.5 km and have an elevation difference of 119 m. It was found that the delay fluctuations between the two sites were statistically similar, and their time series did

not appear to be shifted versions of each other, suggesting that the length scale for evolution of the turbulence pattern is shorter than the separation between instruments. Another significant result was that the fluctuations were slightly weaker at the higher altitude site and consistent with theory [11].

The Venus STI was also involved in a comparison study involving similar data extracted from multifrequency Water Vapor Radiometer (WVR) sky brightness measurements. In August 2008, two WVR units were deployed next to each STI element in an attempt to provide ancillary data that can be used in an intercomparison with the STI phase fluctuations. The sky brightness temperature measurements acquired at different sky frequencies were converted to path delays for each WVR. These path delays were subtracted from each other, yielding a difference data type that was then compared with the concurrent STI path delay for the month of August 2008. The intercomparison study showed that the temporal behavior and the statistics of the two data types were consistent and in reasonable agreement after making the appropriate adjustments [13].

A study involving a comparison between concurrent STI data and arrayed spacecraft signal data at Ka-band received at two Deep Space Network (DSN) antennas within the same complex was also conducted. This study was motivated by NASA's interest in using the technique of arraying smaller diameter antennas to increase effective aperture. Downlink arraying is routinely performed by the DSN at 8.4 GHz (X-band) for certain missions. This technique is expected to be extended to uplink arraying. The received signals from two individual DSN antennas were recorded and processed to obtain independent estimates of interferometer phase to be compared against STI phase after making appropriate adjustments for frequency, elevation angle, and baseline length [14–15].

The fades predicted from the difference of the received phases from the individual stations, DSS-25 and DSS-26, of the Cassini spacecraft's Ka-band signal using open-loop receiver recordings were found to be in good agreement with measured fades from array processing equipment [14–15]. This provided confidence that the two instruments were measuring the same quantity. The amplitude fades estimated from the array processor data were of roughly comparable magnitude as those estimated from the adjusted STI phase data, but their phase time series were not expected to agree since the STI and DSN array were pointed in different directions in the sky. However, the statistics of the STI fade magnitude range were comparable to that of the DSN array. That is, the distribution of the array phase difference estimates extracted from the individual antenna data was found to be statistically similar to the STI phase data (after appropriate adjustments were applied for sky frequency, baseline length, and elevation angle). The individual time series of the two sets of phase fluctuations revealed many features that were correlated, anti-correlated, and time delayed, suggesting the presence of differences in dynamic atmospheric features as the signals propagated across similar and different atmospheric cells.

Kepler spacecraft Ka-band array data over a much longer (~12.5 km) baseline using DSS-25 and another more distant 34-m diameter antenna at Goldstone (DSS-13) validated the thin-screen turbulence model [15].

The phase-delay data have been used to derive refractive index structure parameters C_n^2, which is a measure of the variance of the refractive index over small incremental distances

along the signal path, and therefore is a strong function of water vapor variations at microwave frequencies [16]. A comprehensive study of this parameter was derived from many years of STI measurements that were acquired for the variety of climates represented by these sites. The strongest correlation of C_n^2 measurements with its model occurred for the Goldstone, California site, which represents a high-desert climate. Weaker correlations were found for the Kennedy Space Center site, which represents a subtropical climate. Both Canberra, Australia and Madrid, Spain represent intermediate temperate climate sites. The periods where the strongest correlation was observed were quantified for the Goldstone summers, where the days are typically hot and humid while nights tend to be colder and drier [16].

The significance of the phase-delay statistics presented in this paper can be related to the feasibility of conducting uplink arraying operations by examining derived array loss statistics [17–20]. For downlink arraying, atmospheric phase effects can be removed via processing when there is sufficient strength in the received carrier serving as a reference. However, in the absence of a reference signal such as for uplink arraying, or a weak reference signal for downlink arraying, one needs to rely on factoring in atmospheric array loss in any link predictions. In a previous study, monthly and annual phase-delay statistics were adjusted by element separation, elevation angle, and frequency to yield estimates of array loss for different combinations of 34-m diameter antennas at the Goldstone and Canberra DSN sites [17]. These estimates were presented in tables as a function of availability for both monthly and annual cases. The Madrid results were expected to be similar to those of Canberra. At the X-band uplink frequency of 7.15 GHz, it was found that the array loss at ~99% and 20-deg elevation ran ~0.6 dB for Goldstone and ~1.4 dB for Canberra, making X-band viable for uplink arraying at these two sites. At the Ka-band uplink frequency of 34.5 GHz, it was found that the array loss at ~99% and 20-deg elevation ran ~3 dB or above for both Goldstone and Canberra. Thus, with array loss at 3 dB or higher, one would just revert to using one antenna for uplink. Thus, Ka-band would not be viable for uplink arraying at either Goldstone or Canberra except at the lowest availabilities.

Phase-delay statistics were normalized to a common elevation angle (zenith) using the appropriate adjustment formulation [21] to facilitate intercomparison between sites as discussed in Section IV. For the periodic delivery of these statistics to International Telecommunications Union (ITU) databanks, only adjustments in frequency were performed. The databank submissions are accompanied by a document [21] that provides background information and discusses the data-processing techniques for the application of atmospheric-induced path-length statistics that are provided in ITU Recommendation ITU-R P.311 Databanks [22]. This fascicle [21] provides for information on converting line-of-sight statistics to other elevation angles, element separations, and frequencies for use in array link budgets.

III. Site Characteristics

A general description of the STIs and the use of the extracted phase-delay data were previously provided in Section II. The photos in Figure 1 provide examples of each site's

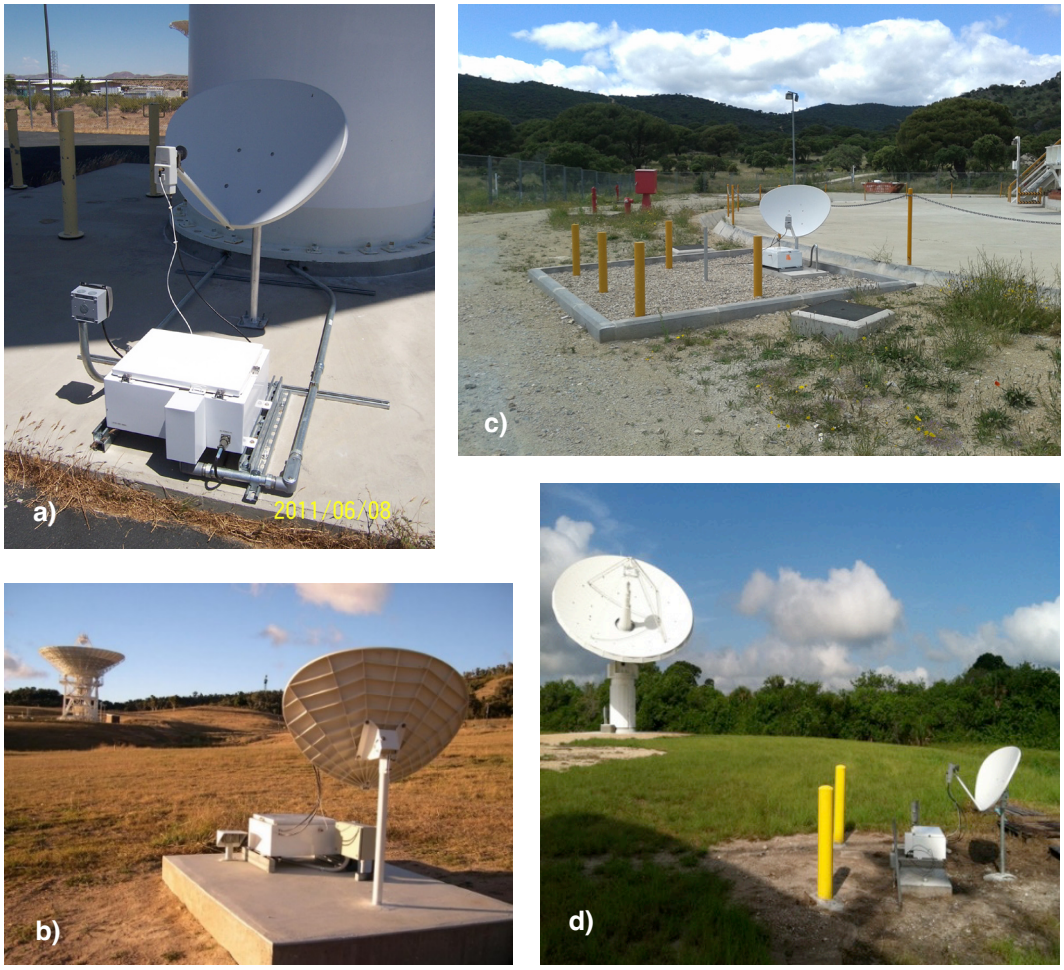

Figure 1. Photos of STI elements at the four sites: a) STI element at Apollo site in Goldstone, California; b) STI element in Canberra, Australia; c) STI element at Madrid, Spain; and d) STI element (foreground) at KSC, Florida, along with one of the larger antennas of the KaBOOM demonstration (background).

terrain along with one of the antenna/electronics box elements. Table 1 specifies key details of each of the STI instruments.

Figure 2 displays the ground layouts for each of the four STI sites along with STI antenna labeling, direction to geostationary satellite serving as the signal source, and nearby infrastructure such as the 34-m beam-waveguide (BWG) antennas of the DSN (Figures 2a [Goldstone], 2b [Canberra], and 2c [Madrid]) and the 12-m diameter antennas of the KaBOOM experiment [4] at KSC (Figure 2d).

The KSC STI used three small (0.8 m) antennas in a triangular configuration with varying spacing of the baselines from 136 to 289 m to receive and process signals from a commercial geostationary satellite (Figure 2d). In contrast, the Canberra STI has nearly identical spacing of its three baselines about 250-m each (see Figure 2b). Although each of the four sites involve three baselines, the phase-delay statistics discussed in Section IV are from one baseline (usually the east–west one) whose lengths are noted in Table 1. In some cases, data from other baselines were used. This was justified based on the finding that the

delay fluctuations between baselines to a given site were statistically similar (other than a small adjustment for baseline length) [12]. A study of the phase-delay data from all three baselines is presented in Section V.

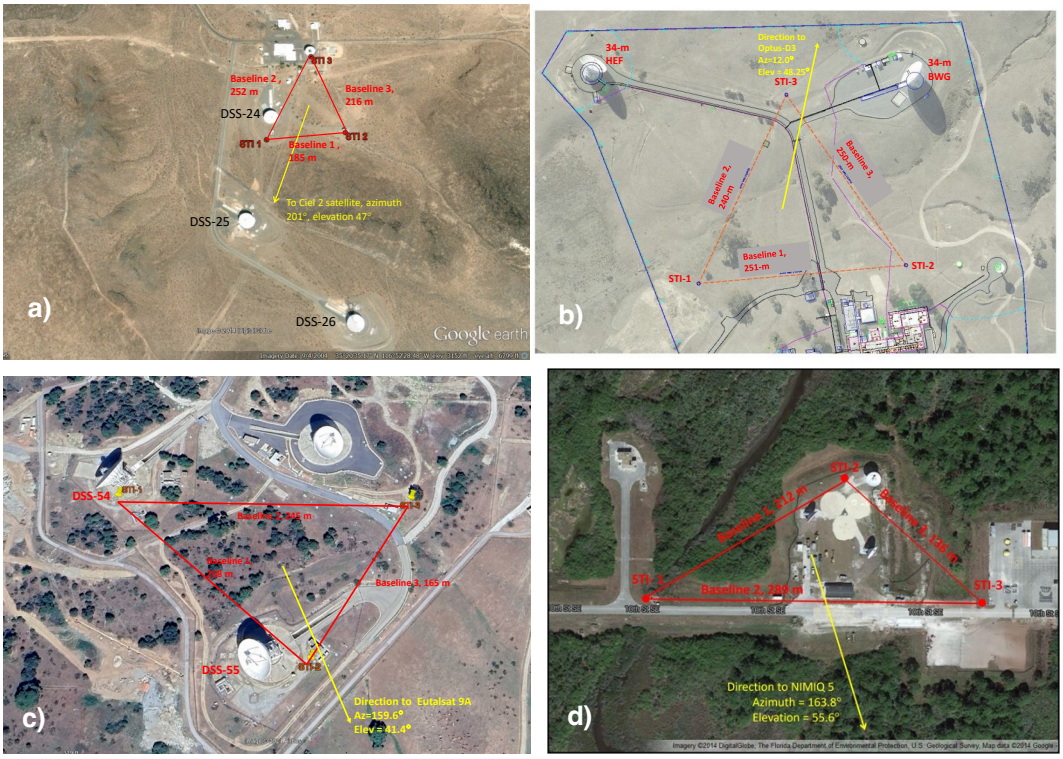

Figure 2. Layouts of the four STI sites showing labeling of each of the STI antennas and direction vectors (azimuth and elevation angle) to the geostationary satellites serving as the signal source for each site: a) Goldstone Apollo, California; b) Canberra, Australia; c) Madrid, Spain; and d) Kennedy Space Center, Florida. Also shown are nearby 34-m diameter antennas for the three DSN sites and the 12-m antennas used for the KaBOOM demonstration [4] at the KSC site, along with control buildings and other facilities. Baseline ground distances between STI elements are shown in red lines annotated with baseline distances.

Table 1. Summary of experiment parameters at each measurement site.

Parameter	Goldstone, CA	Canberra, AUS	Madrid, ESP	KSC, FL
Latitude	35.340 N	35.2 S	40.24 N	28.51 N
Longitude	243.126 E	148.98 E	355.75 E	279.37 E
Altitude	964 m	690 m	830 m	3 m
Baseline Separation(s)	190 m / 252 m (1)	250 m	246 m	191 m
Elevation Angle	47.1°/49.0° (2)	48.2°	41.3°	55.6°
Frequency	12.45 GHz	11.95 GHz	11.95 GHz	12.45 GHz
Satellite	CIEL 2 / ECHOSTAR-7 (2)	OPTUS D3	EUTELSAT 9A	NIMIQ 5
Orbital Position	–129° E / –119° E (2)	156.1° E	9.0° E	287.3° E

The phase-delay data for the Goldstone east–west baseline 1 consisting of elements STI-1 and STI-2 (Figure 2a) was utilized in the study for data acquired from 2011 to November 2019. In November 2019, STI-2 was removed to facilitate the construction of a new 34-m

BWG antenna, designated DSS-23. Since November 2019, data from the one remaining operational baseline consisting of elements STI-1 and STI-3 (Figure 2a) were utilized for the single baseline statistics (see item designated as (1) in Table 1). Satellite Ciel 2 was used as the geostationary satellite signal source from 2011 to August 2023 when it was shut down by the satellite provider. Since August 2023, the signal source was switched to the nearby geostationary satellite Echostar-7 (see items designated as (2) in Table 1).

IV. Single-Baseline Phase-Delay Statistics

The temporal behavior of the phase-delay RMS (in 600 s blocks, each based on 6,000 samples of 0.1 s each) is presented here for each of the four sites for sample winter and summer months. The raw phase RMS values were adjusted to delay RMS values and further adjusted in elevation angle to reference the data to zenith, which is in units of ps.

For the high-desert climate of Goldstone, the phase-delay scatter is typically quiet during the cold winter months (Figure 3a), and more variable and larger during the summer months when it is warmer and more turbulent (Figure 3b). Here the diurnal (day-to-night) signature stands out more clearly during the summer when the peaks occur near local noon (hotter temperature and atmosphere retains more water vapor), whereas during the winter, one could go on for several days without significant variation. During cold months, the strongest fluctuations correspond to the passage of weather systems rather than day-night heating patterns.

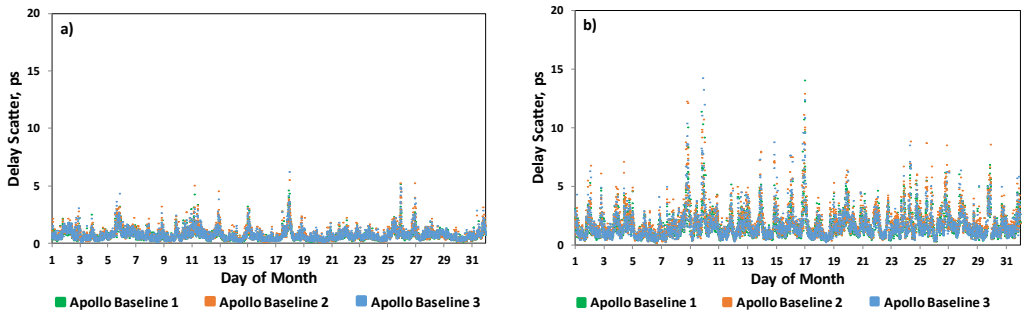

Figure 3. Examples of time series of delay scatter in 600 s intervals for all three Goldstone Apollo baselines, referenced to zenith: a) Sample winter month of December 2018, b) Sample summer month of August 2018. Reprinted from [3].

For the more temperate climate of Canberra, Australia, the phase-delay scatter shown in Figure 4 is not as contrasting between the seasons as it is for Goldstone (Figure 3). One can see significant day-night variation during the southern hemisphere summer (Figure 4a), but with some differences during southern hemisphere winter (Figure 4b) where some features are extended over a few days. The diurnal (day-to-night) signatures stand out more clearly during the summer, whereas during the winter extended features may indicate stormy conditions, with the day-night variation not as evident during other periods.

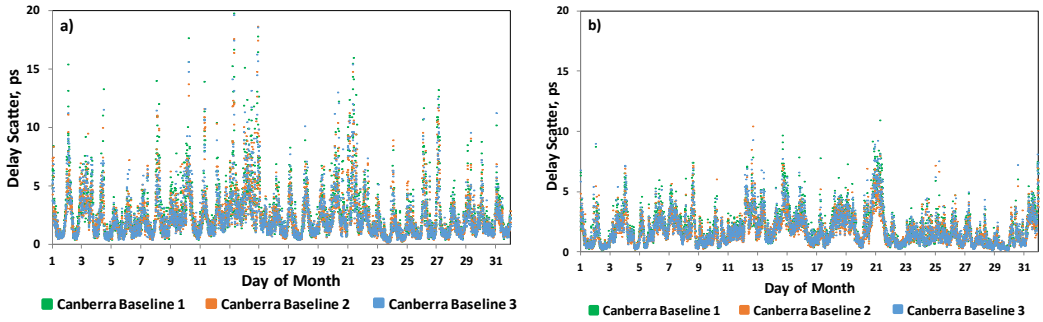

Figure 4. Examples of time series of delay scatter in 600 s intervals for all three Canberra baselines, referenced to zenith: a) Sample summer month of December 2018, b) Sample winter month of August 2018. Reprinted from [3].

For the temperate climate of Madrid, the phase-delay scatter shown in Figure 5 is typically quiet during the cold winter months (Figure 5a), with generally a little more variation when compared with Goldstone winter (Figure 3a). The phase-delay scatter is more variable during the summer months when it is warmer and the climate is more turbulent (Figure 5b), similar with what is seen during Goldstone summer. Note also that the diurnal (day-to-night) signature stands out more clearly during the summer, whereas during the winter, one could go for several days without much discernible variation, similar to what is observed for Goldstone.

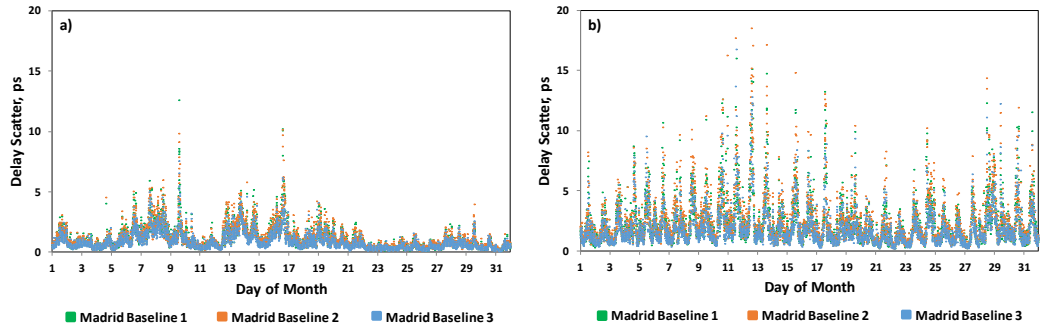

Figure 5. Examples of time series of delay scatter in 600 s intervals for all three Madrid baselines, referenced to zenith: a) Sample winter month of December 2018, b) Sample summer month of August 2018. Reprinted from [3].

For the subtropical climate of KSC, Florida, the difference of phase-delay scatter (Figures 6a and 6b) between seasons is not as extreme as the case for Goldstone (see Figures 3a and 3b). The signature of diurnal variation in phase-delay RMS is more pronounced during summer (Figure 6b) and less pronounced during winter (Figure 6a), but with much higher scatter daytime peaks (for both summer and winter) than for the other sites. It should be emphasized that the data from the KSC STI site have a selection effect in that, during hurricanes, the power to the equipment is shut down.

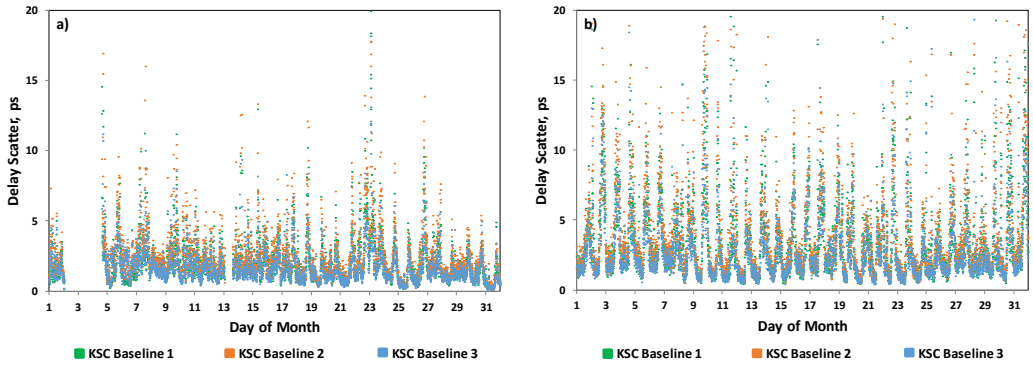

Figure 6. Examples of time series of delay scatter in 600 s intervals for all three Kennedy Space Center baselines, referenced to zenith: a) Sample winter month of January 2017, b) Sample summer month of August 2018. Reprinted from [3].

The coverage of the phase-delay statistics from 2011 to 2018 reported in [3] has been extended to 2023 for this study. The composite monthly and annual path-length exceedance statistics were thus updated and are presented in Figures 7 and 8, respectively. The path-length RMS is referred to line-of-sight (LOS) and its units are given in mm. For context, the magnitude of the path-length delay itself due to water vapor is on the order of a few cm. There is significant variation of the statistics with season, where the curves for the warmer summer months generally lie to the right, the curves for the colder months generally lie to the left, and the curves for the intermediate months (autumn and spring) generally lie in between the winter and summer curves. For the northern hemisphere sites of Goldstone, Madrid, and KSC, the warmer months are usually represented by reddish colors, and for the southern hemisphere site of Canberra, they are represented by bluish colors, where the color schemes are reversed for the colder months. The curves for the intermediate spring and autumn months are usually denoted by yellowish, greenish, and orangish colors.

Figure 7 displays the monthly exceedance statistics of path-delay RMS over 600 s intervals for each of the four sites, which now includes all available data up to the end of 2023. The addition of five more years of data has not changed the results significantly from those presented in the previous study [3], which included data up to the end of 2018. For Goldstone (Figure 7a), the path-length RMS for 0.1% exceedance varies from about 4 mm in summer to about 1.5 mm in winter, making this southwestern desert climate by far the best site in which to conduct arraying. For Canberra (Figure 7b), the path-length RMS at 0.1% exceedance varies from about 6.5 mm in summer to about 3.5 mm in winter. For Madrid (Figure 7c), the path-length RMS at 0.1% exceedance varies from about 5.5 mm in summer to about 2.8 mm in winter. For the subtropical KSC site (Figure 7d), the path-length RMS at 0.1% exceedance varies from about 8 mm in summer to about 4 mm in winter, making this the most variable of the four sites considered.

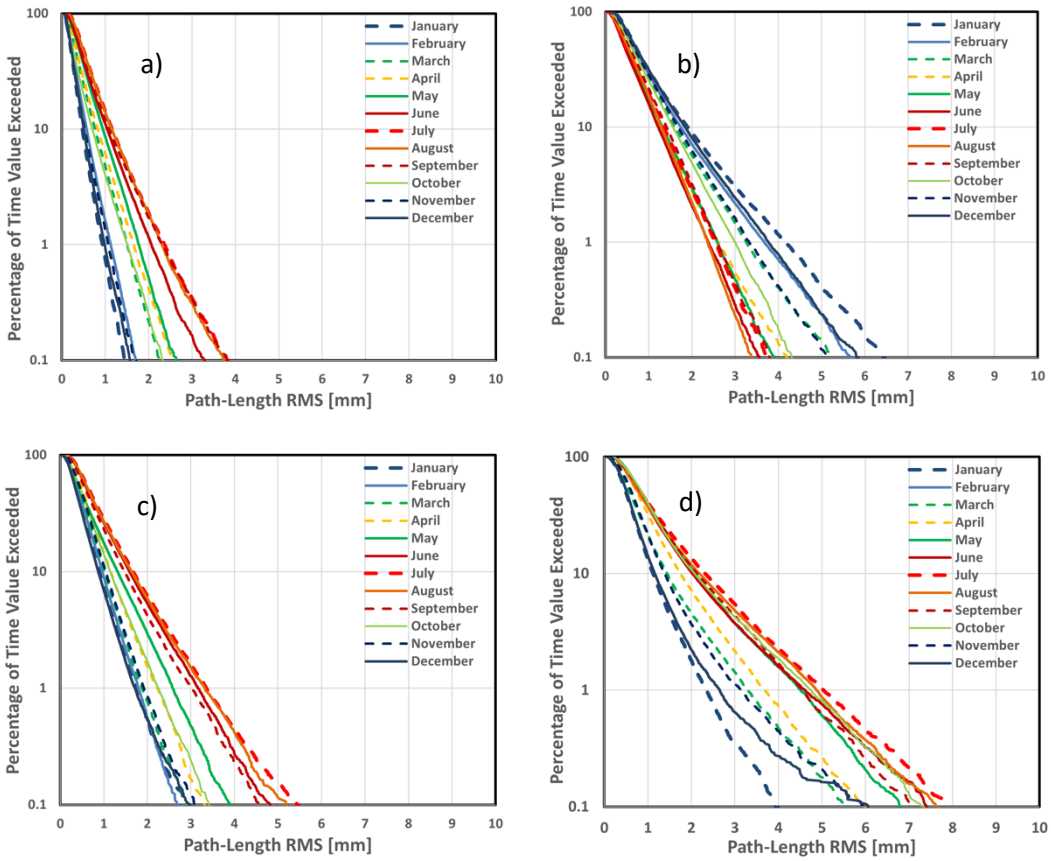

Figure 7. Path-length RMS exceedance statistics for composite months, referenced to LOS: a) Goldstone, b) Canberra, c) Madrid, and d) KSC.

Figure 8 displays the annual exceedance statistics of path-delay RMS over 600 s intervals for each of the four sites. These results have not changed significantly from those presented in the previous study [3], which included data up to the end of 2018. For Goldstone (Figure 8a), the path-length RMS for 0.01% exceedance varies from 4 to 5 mm over the different years from 2011 to 2023, making this "dry" southwestern desert climate by far the best site in which to conduct arraying. For Canberra (Figure 8b), the path-length RMS at 0.01% exceedance varies from about 6 mm to about 7 mm for years 2012 to 2023. For Madrid (Figure 8c), the path-length RMS at 0.01% exceedance varies from about 4.5 mm to about 6.4 mm for years spanning 2014 to March 2023. The apparent outlier curve for Madrid (solid blue in Figure 8c), lying to the left of the other curves, is for a partial year 2023 based on data only from the first three months before a computer hardware failure ceased data acquisition at that site. This is expected as it is biased by cold weather months where phase-delay scatter would be small. For the subtropical KSC site (Figure 8d), the path-length RMS at 0.01% exceedance varies from about 8.4 mm to about 9.8 mm, making this the most problematic of the four sites for arraying.

Figure 9 displays the medians of the annual phase-delay scatter as a function of year for the four STI sites. A linear fit of the values for the Goldstone Apollo STI site (orange circles) produces a trend of 0.0029 mm/yr with an R^2 value of 0.427, suggesting that the measured slope is not statistically significant. As more years of data are acquired, one should be able

to discern whether there is any significance to any increase of phase-delay scatter with year. For context, the mean median phase-delay scatter for Goldstone is 0.32 ± 0.02 mm, where the slope of 0.0029 mm/yr over the 13-year period yields a hypothetical increase of 0.038 mm, almost 2-σ. The average of the Goldstone medians at 0.32 m is the lowest of the four STI sites, with the highest being KSC at ~0.7 mm. Linear fits of the data for the other STI sites show slopes and R^2 values of 0.001 mm/yr and $R^2 = 0.029$ for Canberra, –0.008 mm/yr and $R^2 = 0.38$ for Madrid, and 0.0043 mm/yr and $R^2 = 0.10$ for KSC, respectively. Thus, one could attribute little significance to the linear slopes reported here.

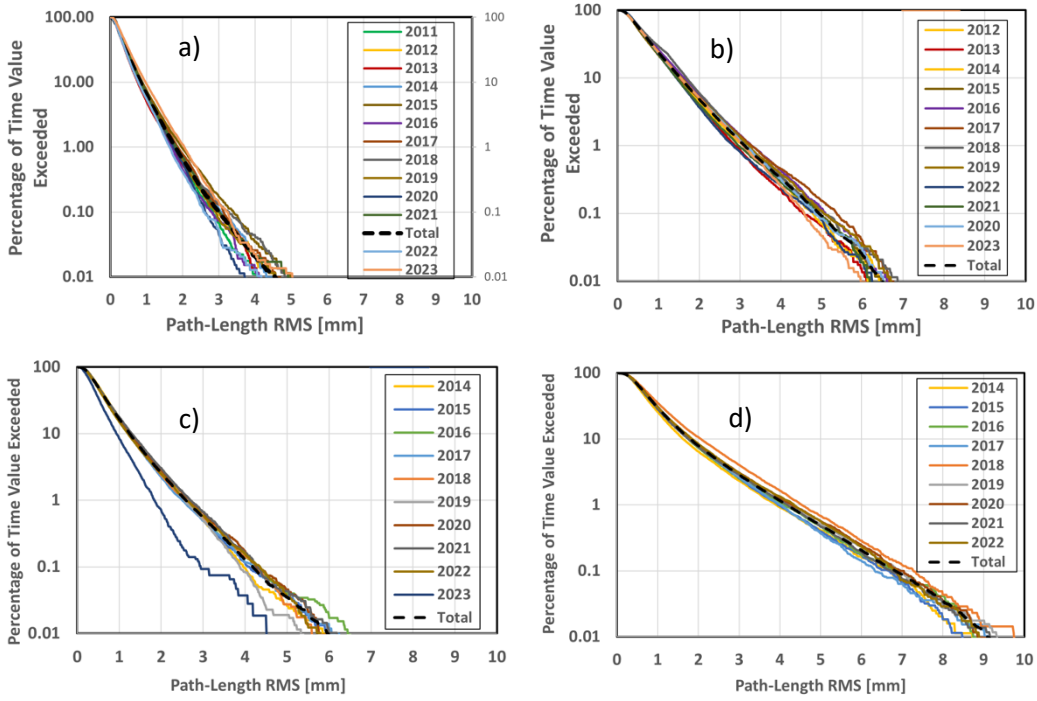

Figure 8. Annual path-length RMS exceedance statistics for different years (solid colors) and for total (dashed black), referenced to LOS: a) Goldstone, b) Canberra, c) Madrid, and d) KSC.

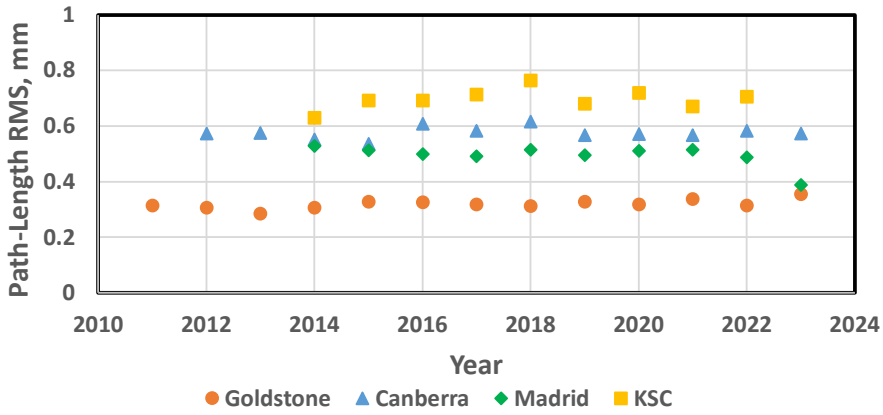

Figure 9. Median values of annual path-length scatter for each of the four STI sites: Goldstone (orange circles), Canberra (blue triangles), Madrid (green diamonds), and KSC (yellow squares).

V. Three-Baseline Phase-Delay Statistics

This section reports on the phase-delay statistics acquired from all three STI baselines when such data exist. Given that σ_1 is the phase-delay scatter of baseline 1 consisting of elements STI-1 and STI-2 (see labels in Figure 2), σ_2 is the phase-delay scatter of baseline 2 consisting of elements STI-1 and STI-3, and σ_3 is the phase-delay scatter of baseline 3 consisting of elements STI-2 and STI-3, we can list the ratios for each of the baseline combinations for each site as shown in Table 2. This table summarizes the results of baseline ratios BL12, BL13, and BL23 averaged over all available three-baseline data up to the end of 2023. Thus, BLij is the ratio of monthly phase-delay scatter of projected baseline i, σ_i, divided by that of the projected baseline j, σ_j as $BLij = \sigma_i/\sigma_j$.

There is a dependence of these phase-delay ratios on the ratios of projected baseline lengths. The measured turbulence has a relationship with the separation distance between elements as the signal propagates through the atmospheric "blobs." The measured values of these ratios can thus be compared against the theoretical values, which have a dependence on projected baseline lengths (r), which are perpendicular to the signal path to the geostationary satellites as $r^{\beta/2}$ [11], where β is taken to be 1.0 (a Kolmogorov slope value intermediate between the thick-layer (5/3) and thin-layer (2/3) model limits). We see reasonable agreement to first order between measured and theoretical values for most of the cases listed in Table 2. One can infer that the scatters in the ratios are on the order of 0.01 to 0.02. In some cases, the difference between measurement and model exceeds 3-sigma.

Discrepancies can be attributed to natural variations, perhaps due to asymmetry from winds and terrain, time-dependent changes in model assumptions (e.g., β), or errors in baseline lengths used in the model due to accuracy of global positioning system (GPS) or surveying measurements.

The ratios of the phase-delay statistics for each month at each site are averaged over all available years of data as shown in Figure 10. Here, one can infer little change versus season for most baselines and sites. For Goldstone (Figure 10a), there are some small increases during the summer months for ratios BL23 and BL13 but not much for ratio BL12. For Canberra (Figure 10b), there are no significant trends with seasons. For Madrid (Figure 10c), there is a hint of an increase in the ratios for BL12 and BL13 during the winter months and insignificant changes for ratio BL23. For KSC (Figure 10d), there is a hint of increase during winter months for ratio BL23.

Table 2. Ratio of phase-delay scatter for three-baseline data.

STI Site		Ratio Baseline 12 σ_1/σ_2	Ratio Baseline 13 σ_1/σ_3	Ratio Baseline 23 σ_2/σ_3	Comments
Goldstone	Measurement	0.894 ± 0.008	0.947 ± 0.015	1.060 ± 0.016	Assumes $\beta = 1$
	Theoretical Model	0.879	0.898	1.02	
Canberra	Measurement	1.101 ± 0.012	1.082 ± 0.007	0.983 ± 0.011	Assumes $\beta = 1$
	Theoretical Model	1.121	1.084	0.967	
Madrid	Measurement	0.912 ± 0.017	1.163 ± 0.019	1.276 ± 0.015	Assumes $\beta = 1$
	Theoretical Model	0.826	1.045	1.265	
KSC	Measurement	0.841 ± 0.012	1.127 ± 0.018	1.342 ± 0.021	Assumes $\beta = 1$, Google Earth coordinates
	Theoretical Model	0.835	1.181	1.414	

Figure 11 displays the monthly averages of the ratios of baseline scatter of all three baselines for a sample winter month (filled circles) and a sample summer month (filled triangles) for all four sites: a) Goldstone, b) Canberra (seasons are reversed in southern hemisphere), c) Madrid, and d) KSC. The like-colors of sample summer and winter months for each site do not always align for a variety of reasons, but are for the most part consistent.

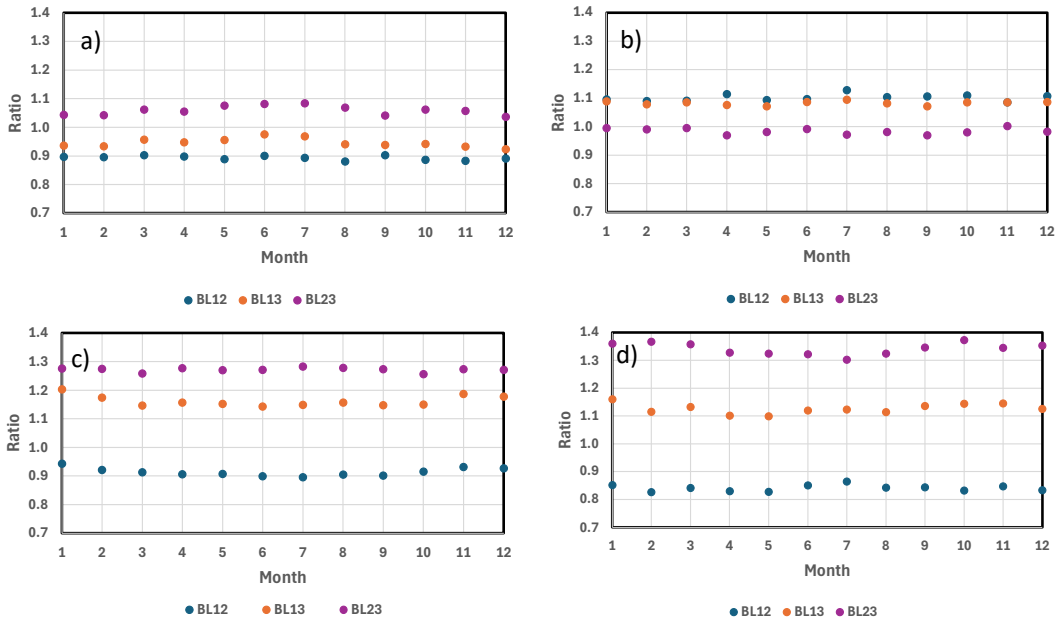

Figure 10. Monthly averages of ratios of phase-delay scatter of all three baselines averaged over all available years of data for each site: a) Goldstone, b) Canberra, c) Madrid, and d) KSC. Months are indicated by the number on the horizontal axes, e.g., 1 for January, 2 for February, etc.

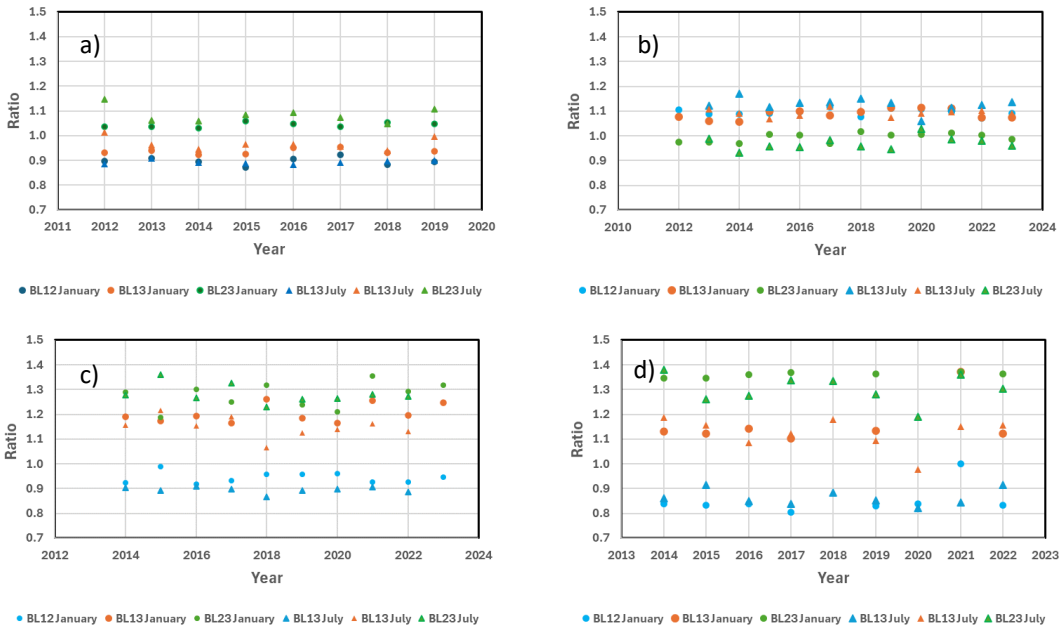

Figure 11. Sample winter month (January) and sample summer month (July) monthly averages of phase-delay scatter ratios as a function of year for all available data for each site; a) Goldstone, b) Canberra, c) Madrid, and d) KSC.

The correlation of these three-baseline (two-dimensional) phase delay statistics with wind speed and wind direction statistics has been identified as work for future study. In the meantime, we present an analysis involving the examination of the correlation of the two-dimensional phase-delay data with wind speed and wind direction for a selected period of data (see Section VI).

VI. Time Series Analysis of Two-Dimensional STI Data with Wind Data

The above study of three-baseline two-dimensional data in Section V involved the examination of time-averaged statistics of the ratios of phase-delay scatter between the three baselines over the available years of data for each STI site. It was found that there was little difference in any temporal changes on the order of monthly or annual timescales between baselines or their ratios, and that the ratios were essentially consistent with those based on theory.

But what about any effects on short timescales based on the short-term temporal phase-delay data itself (not the long-term scatters)? Such analyses could be useful to DSN operations involving multi-element arrays if the effect of strong sustained winds on certain baselines is examined. Here, we follow the methodology presented by Shao et al. [23].

Refer to Figure 12 for a layout of the KSC STIs. For a 10-minute period occurring on August 22, 2013, we see that the wind direction vector (green arrow) is roughly aligned with the flow direction between baseline 1 (STI elements 1 and 2) and baseline 2 (STI elements 1 and 3). This flow direction is indicated by the thick red arrow pointing from the center of baseline 1 to the center of baseline 2 and involves a propagation distance of 59 m (projected relative to direction of signal source).

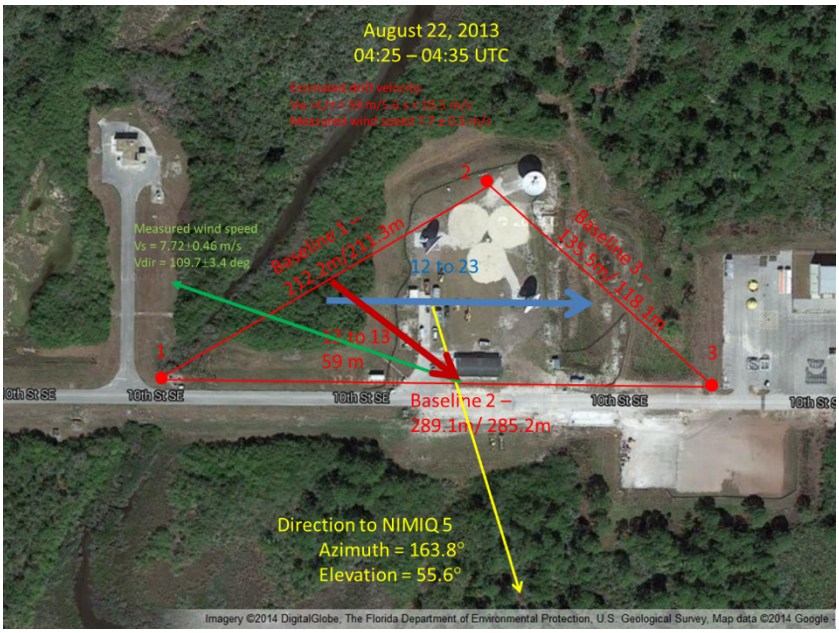

Figure 12. Geometric layout of KSC STI baselines along with annotated element IDs (red), direction to geostationary satellite NIMIQ-5 (yellow arrow), and wind direction vector (green arrow), which indicates 7.72 +/– 0.46 m/s magnitude originating from a 107.9-deg direction.

An inspection of the phase-delay time series shown in Figure 13a indicates a high correction between baseline 1 (black) and baseline 2 (red), consistent with the wind flowing across the two baselines, but significant less correlation with baseline 3 (blue) where the wind direction vector is roughly aligned with the baseline itself. The phase delay from baselines 1 and 2 tends to be highly correlated when the direction of prevailing wind has a significant component flowing across them. The phase delay for baselines 1 and 3 tends to be less correlated as wind direction (green arrow) has a smaller component crossing baseline 3. When the wind velocity vector is aligned with a drift vector, the estimated drift velocity is consistent with the measured wind velocity in both magnitude and direction. Upon inspection of the correlation functions in Figure 13b, we do see that the cross-correlation of baseline 1 with baseline 2 (red curve) is almost aligned with the autocorrelation of baseline 1 (black curve). A close approximation of "eyeballing" the peak of the red curve relative to the black curve shows a delay of about 5.6 seconds. If we estimate the inferred wind speed of the wind traversing baseline 2 to baseline 1, then we get a drift velocity of 59 m/5.6 s = 10.5 m/s, in reasonable agreement with the measured wind speed of 7.7 +/– 0.5 m/s using the 500-ft altitude wind sensor reading on weather tower 0313 at KSC near the STI site [24].

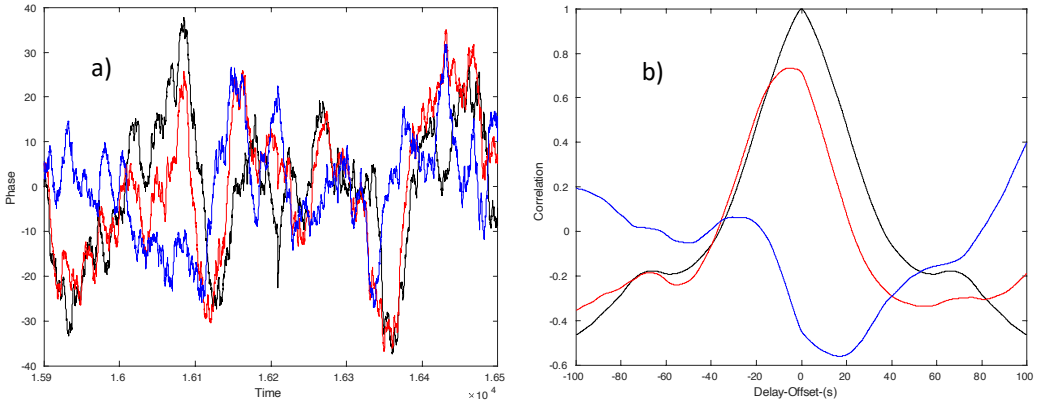

Figure 13. a) Phase delay in deg for each of the three KSC baselines on August 22, 2013, 04:25 to 04:35 UTC, baseline 1 (black), baseline 2 (red), baseline 3 (blue); b) Autocorrelation of baseline 1 (black), cross-correlation of baseline 1 with baseline 2 (red), and cross-correlation of baseline 1 with baseline 3 (blue).

VII. Conclusion

STIs have been operating at the three DSN sites and at KSC for the purpose of gathering statistical data on spatial phase fluctuations induced by the atmosphere. These data are used to characterize the suitability of each site to host potential antenna arrays at high-frequency bands (e.g., Ka-band) for telecommunications and navigation applications. The phase-delay statistics were gathered from the three DSN tracking sites and the KSC site on a monthly and annual basis. The derived statistics are consistent with site climate. The dry desert climate of Goldstone, California, exhibits the lowest annual path-length RMS values, and the subtropical site of KSC in Florida exhibits the highest annual path-length RMS statistics. The path-length statistics for the two DSN tracking sites of Canberra, Australia, and Madrid, Spain, fall in between those of Goldstone and KSC. The phase-delay

scatter between all three baselines for each site have also been examined for consistency and comparison with models. In addition, a short period of phase delay itself from all three baselines of the KSC STI site were examined against wind data, and it was found that there was correlation and consistency with on-site wind sensor data.

Acknowledgments

The support of Stephen Lichten and Douglas Abraham (now retired) of the office of the Interplanetary Network at JPL is very much appreciated. The support provided by the operations crews at each of the DSN tracking sites and at KSC is also appreciated. I would also like to thank Marc Sanchez Net of JPL for providing valuable review comments.

References

[1] R. N. Treuhaft and G. E. Lanyi, "The effect of the dynamic wet-troposphere on radio interferometric measurements," *Radio Science,* vol. 22, no. 2, pp. 251–265, March–April 1987. doi:10.1029/RS022i002p00251. https://agupubs.onlinelibrary.wiley.com/doi/10.1029/RS022i002p00251

[2] D. D. Morabito and L. R. D'Addario, "Site test interferometer atmospheric decorrelation statistics use in uplink array link budgets," *Proceedings of 13th Ka and Broadband Communications Conference,* Turin, Italy, September 24–26, 2007.

[3] D. D. Morabito, "Monthly and annual phase delay statistics acquired from DSN and KSC site test interferometers," *The Interplanetary Network Progress Report,* vol. 42-217, Jet Propulsion Laboratory, Pasadena, California, pp. 1–13, May 15, 2019. https://ipnpr.jpl.nasa.gov/progress_report/42-217/42-217C.pdf

[4] B. Geldzahler, M. Miller, R. Birr, K. Grant, R. Hoblitzell, L. Huddleston, J. Morgan, N. Pack, A. Sherman, G. Woods, V. Vilnrotter, T. Cornish, F. Davarian, D. Lee, D. Morabito, P. Tsao, M. Ott, H. Jakeman, W. J. Thomes, R. Switzer, J. Soloff, S. Chan, and B. Tise, "Field demonstration of coherent uplink from a phased array of widely separated antennas: steps toward a verifiable real-time atmospheric phase fluctuation correction for a high resolution radar system," in *AMOS Conference,* Wailea, Maui, Hawaii, September 9–12, 2014. http://www.amostech.com/TechnicalPapers/2014/Orbital_Debris/GELDZAHLER.pdf

[5] R. J. Acosta, B. Frantz, J. A. Nessel, and D. D. Morabito, "Goldstone site test interferometer," *Proceedings of the 13th Ka and Broadband Communications Conference,* Turin, Italy, September 24–26, 2007.

[6] J. A. Nessel, R. J. Acosta, and D. D. Morabito, "Goldstone site test interferometer phase stability analysis," *Proceedings of the 13th Ka and Broadband Communications Conference,* Turin, Italy, September 24–26, 2007.

[7] R. J. Acosta, J. A. Nessel, I. K. Bibyk, B. Frantz, and D. D. Morabito, "Measurements of k-band carrier amplitude and phase fluctuations due to atmospheric effects via interferometry," *Proceedings of the 12th Ka and Broadband Communications Conference,* Naples, Italy, September 27–29, 2006.

[8] R. J. Acosta, J. A. Nessel, and D. D. Morabito, "Data processing for atmospheric phase interferometers," *Proceedings of the 14th Ka and Broadband Communications Conference,* Matera, Italy, September 24–26, 2008.

[9] J. A. Nessel, R. J. Acosta, and D. D. Morabito, "Phase fluctuations at Goldstone derived from one-year site testing interferometer data," *Proceedings of the 14th Ka and Broadband Communications Conference,* Matera, Italy, September 24–26, 2008.

[10] D. D. Morabito, L. R. D'Addario, S. Shambayati, R. J. Acosta, and J. A. Nessel, "Goldstone site test interferometer atmospheric decorrelation statistics use in spacecraft link budgets: first year of STI data," *Proceedings of the 14th Ka and Broadband Communications Conference,* Matera, Italy, September 24–26, 2008.

[11] D. D. Morabito, L. R. D'Addario, R. J. Acosta, and J. A. Nessel, "Tropospheric delay statistics measured by two site test interferometers at Goldstone, California," *Radio Science,* vol. 48, no. 6, pp. 729–738, November/December 2013. doi:10.1002/2013RS005268. https://agupubs.onlinelibrary.wiley.com/doi/full/10.1002/2013RS005268

[12] D. D. Morabito, L. R. D'Addario, R. J. Acosta, and J. A. Nessel, "An inter-comparison of two independent site test interferometers located in Goldstone, California: initial study results," *Proceedings of the 18th Ka and Broadband Communications, Navigation and Earth Observation Conference,* Ottawa, Canada, September 2012.

[13] D. D. Morabito, L. R. D'Addario, S. Keihm, and S. Shambayati, "Comparison of dual water vapor radiometer differenced path delay fluctuations and site test interferometer phase delay fluctuations over a shared 250-meter baseline," *The Interplanetary Network Progress Report,* vol. 42-188, Jet Propulsion Laboratory, Pasadena, California, pp. 1–21, February 15, 2012. https://ipnpr.jpl.nasa.gov/progress_report/42-188/188A.pdf

[14] D. D. Morabito, L. R. D'Addario, and S. Finley, "A comparison of atmospheric effects on differential phase for a two-element antenna array and nearby site test interferometer," *Radio Science,* vol. 51, no. 2, pp. 91–103, February 2016. doi:10.1002/2015RS005763. https://agupubs.onlinelibrary.wiley.com/doi/10.1002/2015RS005763

[15] D. D. Morabito, L. R. D'Addario, and S. Finley, "Comparison of atmospheric delay statistics from Deep Space Network arrays and nearby site test interferometers," *Proceedings of 22nd Ka- and Broadband Conference,* Cleveland, Ohio, October 17–20, 2016.

[16] D. D. Morabito, L. Wu, and D. Heckman, "Radio refractive index of wet atmosphere estimated from site test interferometer data," *Radio Science,* vol. 57, e2021RS007408, 2022. https://doi.org/10.1029/2021RS007408

[17] D. D. Morabito and L. R. D'Addario, "Atmospheric array loss statistics for the Goldstone and Canberra DSN sites derived from site test interferometer data," *The Interplanetary Network Progress Report,* vol. 42-196, Jet Propulsion Laboratory, Pasadena, California, pp. 1–23, February 15, 2014. https://ipnpr.jpl.nasa.gov/progress_report/42-196/196A.pdf

[18] D. D. Morabito and L. R. D'Addario, "Two-element Uplink Array Loss Statistics derived from site test interferometer phase data for the Goldstone climate: initial study results," *The Interplanetary Network Progress Report,* vol. 42-186, Jet Propulsion Laboratory, Pasadena, California, pp. 1–20, August 15, 2011. https://ipnpr.jpl.nasa.gov/progress_report/42-186/186B.pdf

[19] D. D. Morabito and L. R. D'Addario, "Atmospheric array loss statistics derived from short time scale site test interferometer phase data," *The Interplanetary Network Progress Report,* vol. 42-198, Jet Propulsion Laboratory, Pasadena, California, pp. 1–20, August 15, 2014. https://ipnpr.jpl.nasa.gov/progress_report/42-198/198C.pdf

[20] L. R. D'Addario, "Combining loss of a transmitting array due to phase errors," *The Interplanetary Network Progress Report,* vol. 42-175, Jet Propulsion Laboratory, Pasadena, California, pp. 1–7, November 15, 2008. https://ipnpr.jpl.nasa.gov/progress_report/42-175/175G.pdf

[21] D. D. Morabito and J. Nessel, "Application, validation and data processing of atmospheric path length standard deviation statistics for ground-based antenna array performance predictions," *U.S. Radiocommunication Sector Fact Sheet,* ITU-R Document USWP 3M-9, January 18, 2017.

[22] D. D. Morabito and J. Nessel, "Contributions to the propagation databanks: path length turbulence statistics for Goldstone, CA (Apollo Site); Canberra, AUST; Madrid, Spain; and Kennedy Space Center, Florida," *U.S. Radiocommunication Sector Fact Sheet,* ITU Document USWP 3M-5, January 27, 2017.

[23] X. M. Shao, R. C. Carlos, M. W. Kirkland, C.-Y. J. Kao, and A. R. Jacobson, "Observations of precipitable water vapor fluctuations in convective boundary layer via microwave interferometry," *J. Geophys. Res.,* 104(D14), pp. 16729–16740, 1999. doi:10.1029/1999JD900263.

[24] KSC Spaceport weather data archive site. https://kscweather.ksc.nasa.gov/wxarchive